Energetic and Entropic Contributions to the Surface Energy of a Free-Standing Thin Film of *n*-Tetracontane

Guoqiang Xu and Wayne L. Mattice*

Department of Polymer Science, The University of Akron, Akron, Ohio 44325-3909

Received: June 21, 2002; In Final Form: September 19, 2002

The surface free energy, γ_μ, calculated from the chemical potential, μ, and the contribution of the internal energy to the surface energy, γ_U, are compared for a molecular model of a free-standing thin film of *n*-tetracontane. The coarse-grained chains are represented on a high-coordination lattice with a step length of 2.5 Å. Each occupied site on this lattice represents a two-carbon unit of *n*-tetracontane. The configurations of the coarse-grained chains are governed by two types of energies. Short-range intramolecular conformations are weighted using first- and second-order interactions in the classic rotational isomeric state model of Abe et al. for polyethylene (*J. Am. Chem. Soc*. **1966**, *88*, 631). Intermolecular, as well as long-range intramolecular, interactions are weighted with a discretized Lennard-Jones potential energy function, truncated after the third shell. The contribution of these two energies to γ_U of the amorphous free-standing thin film is 22 erg/cm^2 at 400 K. The chemical potential of the chains in the thin film is evaluated using the chain increment method proposed by Kumar et al. (*Phys. Rev. Lett*. **1991**, *66*, 2935). The analysis of the chemical potential specifies $\gamma_\mu = 20$ erg/cm^2 at 400 K. The estimates of γ_U and γ_μ at this temperature, *T*, differ by about 10%. The small difference in these two values implies that the energetic contributions dominate the entropic contributions to γ_μ of this amorphous free-standing thin film. Both γ_U and γ_μ decrease, at nearly the same rate, when *T* of the simulation rises above 400 K. With a reduction in *T* below 390 K, crystallization of the thin film occurs. The value of γ_U increases as *T* falls below 390 K, reaching 32 erg/cm^2 at 298 K. The usual implementation of the chain increment method for calculating μ becomes unreliable when crystals appear in the thin film.

Introduction

Polymer thin films find uses in an enormous variety of environments. Three types of environments can be defined using the status of the system on either side of the thin film. Often, one side of the thin film is constrained by its attachment or adsorption onto a substrate, while the other side of the film is exposed to air or to a vacuum.[1−15] In another environment, the thin film is confined between two walls.[16] In both of these environments, the nature of the interaction between the polymer and the substrate, or the polymer and the walls, has a significant effect on the properties of the thin film. This effect is eliminated in the third type of environment, which is the free-standing thin film.[17−19] For this reason free-standing thin films play an important role in the development of fundamental knowledge about polymer surfaces. They provide a system where the observable properties are dominated by the inherent behavior of the polymer surface. This inherent behavior is not masked by substrate/polymer interactions that are determined in part by the properties of the substrate.

The experimental study of free-standing polymer thin films is a challenging task, partially because of their mechanical instability. Simulation provides an attractive complimentary approach to the experimental study of these systems, because the periodic boundary conditions employed in a simulation can be chosen so that they suppress mechanical instability.[20] Free-standing thin films have been simulated by a variety of techniques.[20−34] Often, the objectives of the simulation are structural information, such as the density profile; segregation of functional groups or chain ends; or preferred orientations for backbone bonds, side chains, or the radii of gyration tensors of an entire chain. Energetic information, notably an estimate of the surface energy, is also accessible by various techniques. We then confront the issue of whether the quantity calculated does or does not include an entropic contribution. Is it a surface internal energy or a surface free energy, and how strongly do these two energies differ from one another in free-standing polymer thin films?

Here, we calculate both types of surface energies for a model of a free-standing thin film of *n*-tetracontane. The energetic terms, *U*, in the simulation specify a contribution of the internal energy to the surface energy, denoted by γ_U, that can be calculated by a method introduced by Misra et al.[26] Although initially used for atomistically detailed models in continuous space, this method was subsequently shown to be applicable also to coarse-grained models in discretized space.[28] The chain increment method of Kumar et al.[35] is used to estimate the chemical potential, μ, of the chains. This method leads to an estimate of the surface free energy, denoted by γ_μ. The chain increment method has been previously applied[36] to coarse-grained models of polypropylene (PP) chains with different stereochemical compositions that were constructed with the same simulation method[37] as the one employed here for the thin film of *n*-tetracontane. The isothermal, isochoric formation of two-component melts from pairs selected from atactic polypropylene (*a*PP), isotactic polypropylene (*i*PP), and syndiotactic polypropylene (*s*PP) is accompanied by $\Delta\mu > 0$ for the *s*PP chains, but $\Delta\mu$ is not distinguishable from zero for the other two species.[36] This simulation result is consistent with the experimental observations that *a*PP and *i*PP are miscible in the melt,[38] but *s*PP demixes from its melt blends with either of the other two species of PP,[39−41] and with the changes in energy upon mixing evaluated directly from the simulations.[37]

10.1021/jp021470d CCC: $22.00
Published on Web 11/20/2002

The values of γ_U and γ_μ calculated by the two methods differ by no more than 10% when the temperature, T, is chosen so that the thin film of *n*-tetracontane is amorphous. This result implies that entropic effects are dominated by energetic effects in the surface region of an amorphous free-standing thin film of this alkane. Both γ_U and γ_μ decrease with increasing T when the film is amorphous. The values of γ_U increase when T falls below the melting temperature, T_m. The usual implementation of the chain increment method appears to have some difficulty in the calculation of γ_μ when $T < T_m$.

Simulation Method and Details

The structures of the equilibrated replicas of free-standing thin films of *n*-tetracontane were described recently.[33] The system contains 155 independent coarse-grained parent chains (N_c), each represented by 20 beads (N) on a high-coordination lattice. Use of a single bead for each two-carbon unit provides a computational advantage over conventional united-atom (one bead for each carbon atom) and fully atomistic models. The periodic box has 24 steps (of length 2.5 Å) in the x and y directions. The number of steps along the z axis (perpendicular to the surface) is so large that the chains cannot interact with their images in this direction. The chains can be reverse-mapped to $C_{40}H_{82}$ in continuous space.[42] The short-range intramolecular interactions of the beads are obtained by mapping the rotational isomeric state (RIS) model of Abe et al.[43] for polyethylene (PE) onto the coarse-grained description of the chains. The intermolecular interactions and long-range intramolecular interactions are described by a discretized Lennard-Jones (LJ) potential. The discretization employs the Mayer f function to enforce identical values for the second virial coefficient of a nonideal gas described by the continuous LJ potential function with $\epsilon/k_B =$ 185 K and $\sigma = 4.4$ Å and by the discretized function used on the high-coordination lattice.[44] k_B denotes Boltzmann's constant. This set of parameters has been used previously in simulations of PE melts,[45] thin films,[28,34] nanofibers above T_m,[46] and bulk *n*-tetracontane below T_m.[47] The energies in the first two shells are repulsive, and the strongest attraction appears in the third shell. At 400 K, the discretized energies for the first three shells are 12.835, 0.388, and −0.630 kJ/mol, respectively.[33] The energies in the fourth and higher shells are less strongly attractive than the energy in the third shell. Ignoring these higher shells speeds the simulation,[48] with little sacrifice in the quality of the models that are produced.

The thin film crystallizes below 390 K.[33] Two types of crystalline configurations can be obtained in independent quenches from the amorphous region. One configuration has a grain boundary in the center of the thin film. There are two differently oriented crystals on either side of the grain boundary. The other configuration crystallizes completely, with no residual grain boundary in the middle of the thin film. Annealing at a temperature slightly below T_m demonstrated that the more stable structure is the one without the grain boundary.[33] The crystalline thin films used in the present study are those without the grain boundary.

Each thin film is free to select its plateau density in the interior, ρ_B, as well as its density profile, $\rho(z)$, in the surface region. The z axis is normal to the surface of the thin film. At a particular T, the density, ρ, at the surface decays with a profile, $\rho(z)$, described by the usual hyperbolic tangent function

$$\rho(z) = (\rho_B/2)[1 - \tanh(z/\xi)] \quad (1)$$

During the fitting procedure, the zero for z is translated to the point where $\rho(z) = \rho_B/2$. The value of ξ, which is a measure of the width of the surface region, is about 6 Å when the thin film is amorphous. The value of ξ is smaller by a factor of 3 when the film is crystalline.[33] The heat (2.5 kJ mol^{-1}) and entropy (7.9 J K^{-1} mol^{-1}) of fusion evaluated from the simulation[33] fall within the ranges reported for PE (1.45−3.73 kJ mol^{-1} and 3.5−8.9 J K^{-1} mol^{-1}, respectively[49]).

When the material of interest can be represented by a fluid composed of spherical particles, Widom's test-particle method is often used for evaluation of the residual chemical potential, which is denoted by μ_r.[50] This term is related to μ by

$$\mu = \mu_r + \mu^{i0} \quad (2)$$

Here, μ^{i0} denotes the chemical potential of the particle in the ideal-gas state at the same ρ and T as the fluid. The residual chemical potential is obtained from the energy, U_t, of the interaction of a test particle that is randomly inserted into a previously equilibrated fluid of N particles

$$-\beta\mu_r = \ln[\langle \exp(-\beta U_t)\rangle]_N \quad (3)$$

Here, $\beta = 1/k_B T$ and the angle brackets denote the canonical ensemble average.

This method is not easily applied to dense amorphous macromolecules because nearly all of the attempted insertions of a long test chain produce unacceptable overlap with other molecules, causing U_t to be operationally indistinguishable from infinity. The chain increment method of Kumar et al. alleviates this problem.[35] An arbitrarily selected chain end is extended by one monomer unit, and this new monomer unit is used as a test bead. The energy of the interaction of this test bead with the previous components of the system, which do not change their coordinates in response to the test bead, is denoted by $U_{t,test}$. It is related to the residual chemical potential of the test bead, $\mu_{r,test}$, by

$$-\beta\mu_{r,test} = \ln[\langle \exp(-\beta U_{t,test})\rangle]_N \quad (4)$$

The residual chemical potential of the entire chain is approximated as the product of its degree of polymerization and $\mu_{r,test}$ for the test bead[51,52]

$$\mu_r = N\mu_{r,test} \quad (5)$$

The chain increment method has been demonstrated to work successfully for melt blends constructed with the type of simulation employed in the present work.[36]

In the present calculations with these replicas of the free-standing thin film, the values of $U_{t,test}$ are obtained as

$$U_{t,test} = U_{t,RIS} + U_{t,LJ} \quad (6)$$

where $U_{t,RIS}$ is the difference in the RIS energy of a previously existing chain of 20 beads and the RIS energy of this chain after it is extended by one bead. The LJ interaction of the new bead with other beads in its first three shells is denoted by $U_{t,LJ}$, except that we avoid double counting of its short-range intramolecular interactions with those beads that were evaluated separately by the RIS model.

Results and Discussion

We first describe the results obtained with the amorphous thin film at 400 K, which is slightly above T_m. Then, we consider the effect of an increase in T for the amorphous film. Finally, we consider systems with $T = 390$ K or lower, where the thin film contains crystals.

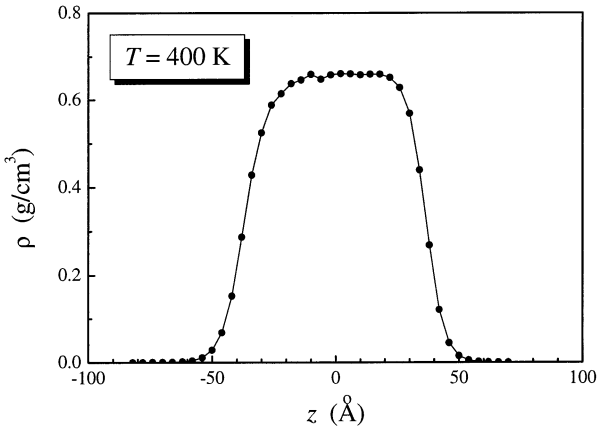

Figure 1. Density profile normal to the surface for the amorphous free-standing thin film of *n*-tetracontane at 400 K.

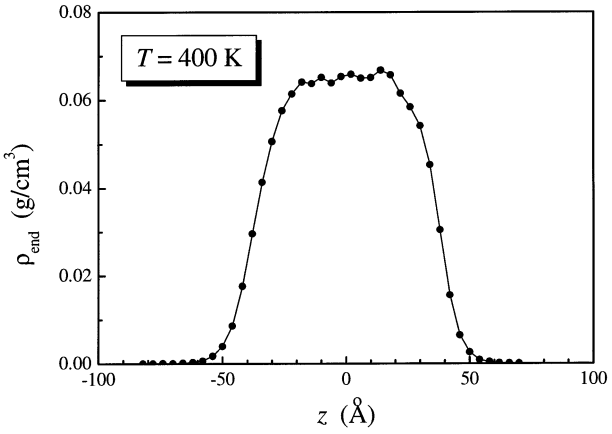

Figure 2. Density profile for the chain ends of the amorphous free-standing thin film of *n*-tetracontane at 400 K.

The Amorphous Thin Film at 400 K. Figure 1 depicts the density profile for the thin film at 400 K, in the direction normal to the surface. The zero for z in this figure is defined so that it includes the center of mass of the thin film. Bins of 4 Å width are used for z. The interior of the thin film has a plateau density of about 0.65 g/cm^3, which is a reasonable density for bulk *n*-tetracontane at this temperature.[53] The density profile for the beads at the chain ends, Figure 2, has nearly the same shape. A very close comparison of the density profiles in Figures 1 and 2 reveals a slight tendency for segregation of the chain ends in the low-density surface region.

Figure 3 depicts the values of $\langle \exp(-\beta U_{t,test}) \rangle$, calculated for extensions of chain ends located in narrow bins centered on the specified value of z. These averages determine the local value of $\mu_{r,test}$ via eq 4. They exhibit a plateau in the interior of the thin film and decrease as one moves into the regions of the thin film where ρ decreases. The scatter in the data is large when the absolute value of z is also large. This increased scatter is due to the small number of observations, which is evident from the values of ρ_{end} in these regions in Figure 2.

The origin of the decrease in $\langle \exp(-\beta U_{t,test}) \rangle$ in the wings of Figure 3 is revealed by separate consideration of the average contributions of the RIS energy and LJ energy to the insertion energies. These data are depicted in Figure 4. Because the ultimate interest is in the difference in the chemical potential in two environments, the changes in the average energies with z are pertinent, but the reference points for calculating the individual energies are irrelevant. Both average energies are constant in the region where ρ is very close to ρ_B. As one moves into the region where ρ decreases, any tendency for a change

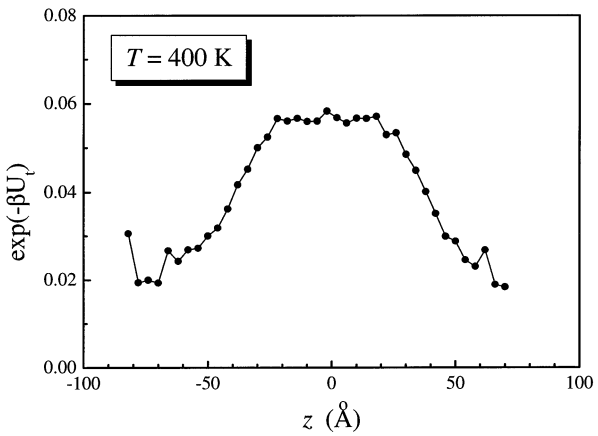

Figure 3. Values of $\langle \exp(-\beta U_t) \rangle$ at 400 K for extensions at chain ends using 4 Å bins for z, the normal to the surface.

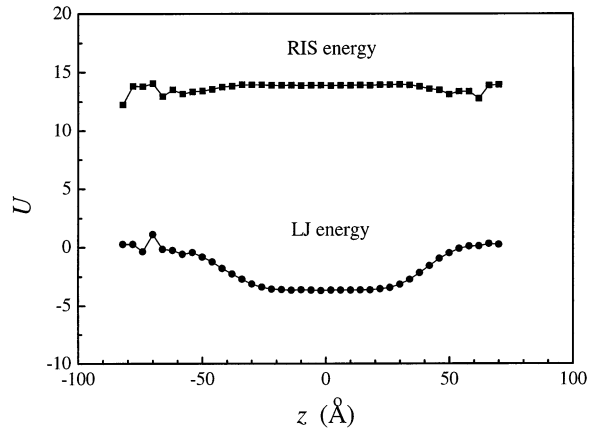

Figure 4. Average values of the RIS and LJ contributions to the extension energies, in kJ/mol, for extensions at chain ends at 400 K. The chain ends are grouped in 4 Å bins for z.

in the RIS contribution to the insertion energy with z is obscured by the increased scatter in the data. In contrast, the LJ contribution to the insertion energy exhibits a systematic increase upon passing from the internal region with $\rho \approx \rho_B$ to the low-density region where $\rho < \rho_B$. This increase in LJ energy must arise because the number of existing beads in a third-shell occupancy (where the discretized LJ interaction is attractive) for a newly inserted bead is larger if insertion occurs near the center of the film than if insertion takes place in the surface region.

An estimate of γ_μ can be extracted from the data depicted in Figure 3. First, we consider only those extensions that occur in the internal plateau region, which is defined for this purpose to be from $z = -15$ to $z = 15$ Å. Similar results are obtained if the internal plateau region is defined to lie between $z = -10$ to $z = 10$ Å. When $\langle \exp(-\beta U_{t,test}) \rangle$ is evaluated using just the chain ends located in this region, its use in eqs 4 and 5 gives a value of $\mu_{r,bulk,test}$ of 9.590 kJ/mol. A slightly different result is obtained for $\langle \exp(-\beta U_{t,test}) \rangle$ when this quantity is averaged over all chain extensions, regardless of the position of the chain end at which the extension occurs. Use of this value of $\langle \exp(-\beta U_{t,test}) \rangle$ in eqs 4 and 5 specifies the value of $\mu_{r,film,test}$ of 9.834 kJ/mol. The change in chemical potential for transferring a chain from the bulk to the thin film is $(\mu_{r,film,test} - \mu_{r,bulk,test})N$. The standard deviation of $\mu_{r,film,test} - \mu_{r,bulk,test}$ is about 0.005 kJ/mol. The simulation uses N_c independent parent chains, and the surface area of the thin film, denoted by A, is determined from the periodic boundary conditions to be 6235 Å^2. Therefore, the

surface free energy in the simulation is 20.1 erg/cm^2, calculated according to

$$\gamma_\mu = A^{-1}(\mu_{\mathrm{r,film,test}} - \mu_{\mathrm{r,bulk,test}})\,NN_\mathrm{c} \tag{7}$$

Alternatively, we can calculate the average of the sum of the RIS and LJ energies for beads in the bulk region (again taken from $z = -15$ to $z = 15$ Å) and also calculate the average of these energies regardless of the location of the beads. The insertion of a test bead is not required for these calculations. These two averages, $U_{\mathrm{r,bulk}}$ and $U_{\mathrm{r,film}}$, are 6.005 and 6.268 kJ/mol, respectively. The contribution of these energies to the surface energy

$$\gamma_\mathrm{U} = A^{-1}(U_{\mathrm{r,film}} - U_{\mathrm{r,bulk}})\,NN_\mathrm{c} \tag{8}$$

specifies a value of 21.6 erg/cm^2. Therefore, the change in chemical potential, eq 7, and change in internal energy, eq 8, specify nearly the same value for the surface energy. Of course, $\Delta\mu$ includes the $T\Delta S$ term, where S is the entropy, but this term is absent in ΔU. Therefore, the contribution of $T\Delta S$ to γ_μ cannot be more than approximately 10% of the total, because $(\gamma_\mathrm{U} - \gamma_\mu)/\gamma_\mu \approx 0.1$. The present results for *n*-tetracontane do not permit a statement about whether this value of $(\gamma_\mathrm{U} - \gamma_\mu)/\gamma_\mu$ has a dependence on the degree of polymerization of the alkane.

An independent estimate of the expected surface tension of *n*-tetracontane at 400 K suggests that the results from simulation might be low by 10−20%. The independent estimate starts with data tabulated by Owen for linear PE with a M_W of 67 000 g/mol.[54] These data yield an estimate of 30 erg/cm^2 for the surface tension of PE at 400 K. The influence of molecular weight is estimated using the equation of LeGrand and Gaines[55]

$$\gamma_\mathrm{M} = \gamma_\infty - K/M^{2/3} \tag{9}$$

with the value of K approximated using the result for PE and an assumed surface tension of 17 erg/cm^2 for tridecane at 400 K. The estimate for tridecane is based on extrapolation to 400 K of experimental data for this alkane at 300 and 350 K.[30] This procedure produces an estimate of 24 erg/cm^2 for the surface tension of *n*-tetracontane at 400 K, which is slightly larger than the γ_μ and γ_U values from the simulation.

Previous molecular dynamics simulations of tridecane using explicit-atom and united-atom force fields yielded surface energies of 18.72 and 19.12 erg/cm^2, respectively, at 400 K.[30]

Temperature Dependence of the Surface Energies. The temperature dependence of γ_U and γ_μ from the simulation is presented in Figure 5. We consider first the results for the temperature range 400−475 K, where the free-standing thin film is amorphous. Throughout this range, γ_U and γ_μ are nearly indistinguishable. The line inserted above the data has a slope of −0.057 (erg/cm^2)/K, which is the value of the temperature coefficient tabulated for liquid PE by Owen.[54] A line with this slope is a plausible description of the simulated data for *n*-tetracontane above 400 K.

The simulation finds that the thin film is amorphous at 400 K, but it is highly crystalline at 390 K.[33] The data in Figure 5 show that γ_U and γ_μ increase upon cooling from 400 to 390 K, but the increase is no greater than a factor of 1.1. As the crystalline thin film is cooled from 390 to 298 K, γ_μ from the simulation increases at a faster rate than does γ_U. The values for γ_U seem to be closer to expectation. Owen, for example, tabulates a surface tension of 33 erg/cm^2 for solid PE.[54] At 298 K, γ_U from the simulation is about 32 erg/cm^2, but application of the chain increment method yields a value for γ_μ of 43 erg/cm^2.

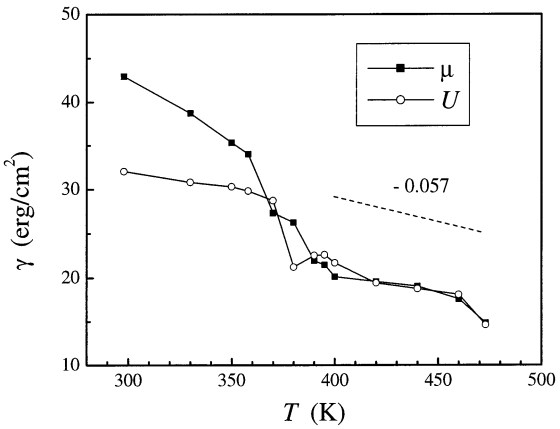

Figure 5. Values of γ_U and γ_μ estimated from the simulations of the free-standing thin films of *n*-tetracontane at various values of T. The T_m of the thin film in the simulation is 390 K.[33] The dashed line above T_m is drawn with a slope of −0.057 (erg/cm^2)/K. The crystalline models used at $T \leq T_\mathrm{m}$ do not have a grain boundary in the interior of the film.

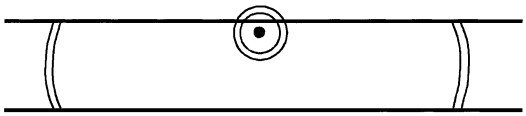

Figure 6. Two thin spherical shells (circular in the two-dimensional representation in the figure) drawn at large and small radii about an arbitrarily chosen site in a thin film.

The Chain Increment Method in the Amorphous and Crystalline Films. The behavior of γ_U and γ_μ over the temperature range 298−475 K prompts an examination of the chain increment method, to determine whether the accuracy of the μ obtained by this method might depend on the choice of T within this range. Inaccuracy has been reported previously upon the application of Widom's test-particle method to an inhomogeneous system composed of a Lennard-Jones fluid in a pore.[56] The parameters in this simulation are appropriate for argon in a cylindrical pore of carbon. Inaccurate values for the chemical potential were obtained for the argon atoms in the region very close to the wall. The inaccuracy was attributed to the high local density in this region.[56]

The present application to thin films is sketched in Figure 6. If a spherical shell with a small radius is drawn about a reference bead in the simulation, the number of other beads in this shell might depend on the local density of the thin film about the reference bead, and the result might depend on the choice of the reference bead. On the other hand, if the radius of the shell is sufficiently large, the result must become independent of the selection of the reference bead. An analogy to a pair correlation function counts the average number of beads in various shells, using internal and end beads as the reference. Both pair correlation functions are normalized so that they approach a value of 1 as the shell number becomes large.

The pair correlation functions defined and normalized in this manner are depicted in Figure 7. In the amorphous thin film at 400 K, nearly identical results are obtained with end and inner beads as references. This behavior is consistent with the fact that density profiles for all beads (Figure 1) and end beads (Figure 2) have nearly the same shape. To see that there is some segregation of end beads near the surface, one needs to examine the ratio of the two densities as a function of z.[28] The

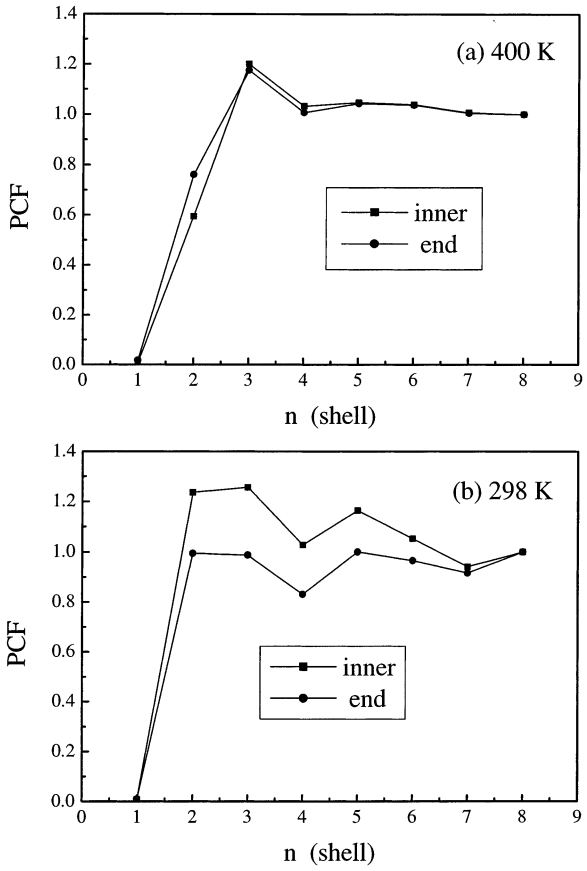

Figure 7. Normalized pair correlation functions (as defined in the text) about inner and end beads (a) in the amorphous *n*-tetracontane thin film at 400 K and (b) in the crystalline *n*-tetracontane thin film at 298 K.

strong similarity in the two pair correlation functions in Figure 7a is consistent with the expectation that similar results would be obtained for insertion of the test bead at a chain end or at an internal site within the chain, $\langle \exp(-\beta U_{\mathrm{t,test,end}})\rangle = \langle \exp(-\beta U_{\mathrm{t,test,internal}})\rangle$, which justifies the calculation of μ_{r} for the chains as $N\beta^{-1} \ln[\langle \exp(-\beta U_{\mathrm{t,test,end}})\rangle]$.

Figure 7b shows that the development of significant structure within the thin film, by crystallization at 298 K, causes the normalized pair correlation functions to depend on the position of the reference bead within the chain. Inner beads have more beads located about them in shells 2−6 than do end beads. This result implies that $\langle \exp(-\beta U_{\mathrm{t,test,end}})\rangle \neq \langle \exp(-\beta U_{\mathrm{t,test,internal}})\rangle$. At 298 K, it is no longer appropriate to identify μ_{r} for the entire chain with $N\beta^{-1} \ln[\langle \exp(-\beta U_{\mathrm{t,test,end}})\rangle]$. Therefore, the customary application of the chain increment method produces inaccurate results for γ_μ at $T < T_{\mathrm{m}}$, although the same method produces reliable results for γ_μ at $T > T_{\mathrm{m}}$. The inaccuracy in the present simulation is produced by crystallization of the chains used in the simulation, whereas the inaccuracy in the simulation[56] of argon in a carbon pore was produced by adhesion of the argon to the surface of the carbon pore, thereby producing an increase in the local density of argon.

Conclusion

Models for the amorphous free-standing thin films of *n*-tetracontane produce surface energies, and temperature coefficients for these surface energies, that are within about 10% of estimates from experimental data. The surface internal energy, γ_{U}, and surface free energy, γ_μ, differ by only about 10% in the simulation, which implies that the contribution from the internal energy dominates the contribution from the entropy. The models of the amorphous thin films have nearly the same shape for density profiles calculated using all beads and end beads.

When the temperature of the simulation is decreased to $T < T_{\mathrm{m}}$, there is an increase in γ_{U}. The value of γ_μ becomes unreliable, because of a breakdown in the procedure for the conversion from the residual chemical potential of a test bead to the residual chemical potential of an entire chain.

Acknowledgment. This work was supported by Grant DMR 0098321 from the Polymer Program at the National Science Foundation.

References and Notes

(1) Zhao, W.; Zhao, X.; Rafailovich, M. H.; Sokolov, J.; Composto, R. J.; Smith, S. D.; Satkowski, M.; Russell, T. P.; Dozier, W. D.; Mansfield, T. *Macromolecules* **1993**, *26*, 561.
(2) Keddie, J. L.; Jones, R. A. L.; Cory, R. A. *Europhys. Lett.* **1994**, *27*, 59.
(3) Elman, J. F.; Johs, B. D.; Long, T. E.; Koberstein, J. T. *Macromolecules* **1994**, *27*, 5341.
(4) Hopkinson, I.; Kiff, F. T.; Richards, R. W.; Affrossman, S.; Hartshorne, M.; Pethrick, R. A.; Munro, H.; Webster, J. R. P. *Macromolecules* **1995**, *28*, 627.
(5) Frank, B.; Gast, A. P.; Russell, T. P.; Brown, H. R.; Hawker, C. *Macromolecules* **1996**, *29*, 6531.
(6) van Zanten, J. H.; Wallace, W. E.; Wu, W. *Phys. Rev. E* **1996**, *53*, R2053.
(7) Hall, D. B.; Hooker, J. C.; Torkelson, J. M. *Macromolecules* **1997**, *30*, 667.
(8) Tanaka, K.; Takahara, A.; Kajiyama, T. *Macromolecules* **1997**, *30*, 6626.
(9) Satomi, N.; Takahara, A.; Kajiyama, T. *Macromolecules* **1999**, *32*, 4474.
(10) Brûlet, A.; Boué, F.; Menelle, A.; Cotton, J. P. *Macromolecules* **2000**, *33*, 997.
(11) Schwab, A. D.; Agra, D. M. G.; Kim, J.-H.; Kumar, S. K.; Dhinojwala, A. *Macromolecules* **2000**, *33*, 4903.
(12) Gautam, K. S.; Schwab, A. D.; Dhinojwala, A.; Zhang, D.; Dougal, S. M.; Yeganeh, M. S. *Phys. Rev. Lett.* **2000**, *30*, 3854.
(13) Fryer, D. S.; Nealey, P. F.; de Pablo, J. J. *Macromolecules* **2000**, *33*, 6439.
(14) Jones, R. L.; Kumar, S. K.; Ho, D. L.; Briber, R. M.; Russell, T. P. *Macromolecules* **2001**, *34*, 559.
(15) Fryer, D. S.; Peters, R. D.; Kim, E. J.; Tomaszewski, J. E.; de Pablo, J. J.; Nealey, P. F.; White, C. C.; Wu, W. *Macromolecules* **2001**, *34*, 5627.
(16) Drummond, C.; Israelachvili, J. *Macromolecules* **2000**, *33*, 4910.
(17) Forrest, J. A.; Dalnoki-Veress, K.; Stevens, J. R.; Dutcher, J. R. *Phys. Rev. Lett.* **1996**, *77*, 2002.
(18) Mol, E. A. L.; Wong, G. C. L.; Petit, J. M.; Rieutord, F.; de Jeu, W. H. *Phys. Rev. Lett.* **1997**, *79*, 3439.
(19) Shin, K.; Pu, Y.; Rafailovich, M. H.; Sokolov, J.; Seeck, O. H.; Sinha, S. K.; Tolan, M.; Kolb, R. *Macromolecules* **2001**, *34*, 5620.
(20) Mansfield, K. F.; Theodorou, D. N. *Macromolecules* **1990**, *23*, 4430.
(21) Madden, W. G. *J. Chem. Phys.* **1987**, *87*, 1405.
(22) Theodorou, D. N. *Macromolecules* **1989**, *22*, 4589.
(23) Mansfield, K. F.; Theodorou, D. N. *Macromolecules* **1991**, *24*, 6283.
(24) Harris, J. G. *J. Phys. Chem.* **1992**, *96*, 5077.
(25) Kumar, S. K.; Russell, T. P.; Hariharan, A. *Chem. Eng. Sci.* **1994**, *49*, 2899.
(26) Misra, S.; Fleming, P. D., III.; Mattice, W. L. *J. Comput.-Aided Mater. Des.* **1995**, *2*, 101.
(27) Curro, J. G.; Weinhold, J. D.; McCoy, J. D.; Yethiraj, A. *Comput. Theor. Polym. Sci.* **1998**, *8*, 159.
(28) Doruker, P.; Mattice, W. L. *Macromolecules* **1998**, *31*, 1418.
(29) Ito, M.; Matsumoto, M.; Doi, M. *Fluid Phase Equilib.* **1998**, *144*, 395.
(30) Chang, J.; Han, J.; Yang, L.; Jaffe, R. L.; Yoon, D. Y. *J. Chem. Phys.* **2001**, *115*, 2831.
(31) Clancy, T. C.; Jang, J. H.; Dhinojwala, A.; Mattice, W. L. *J. Phys. Chem. B* **2001**, *105*, 11493.
(32) Jain, T. S.; de Pablo, J. J. *Macromolecules* **2002**, *35*, 2167.
(33) Xu, G.; Mattice, W. L. *J. Chem. Phys.* **2002**, *116*, 2277.
(34) Doruker, P.; Mattice, W. L. *Macromolecules* **1999**, *32*, 194.
(35) Kumar, S. K.; Szleifer, I.; Panagiotopoulos, A. Z. *Phys. Rev. Lett.* **1991**, *66*, 2935.
(36) Xu, G.; Clancy, T. C.; Mattice, W. L.; Kumar, S. K. *Macromolecules* **2002**, *35*, 3309.

(37) Clancy, T. C.; Pütz, M.; Weinhold, J. D.; Curro, J. G.; Mattice, W. L. *Macromolecules* **2000**, *33*, 9452.
(38) Lohse, D. J. *Polym. Eng. Sci*. **1986**, *26*, 1500.
(39) Thomann, R.; Kressler, J.; Setz, S.; Wang, C.; Mülhaupt, R. *Polymer* **1996**, *37*, 2627.
(40) Thomann, R.; Kressler, J.; Rudolf, B.; Mülhaupt, R. *Polymer* **1996**, *37*, 2635.
(41) Maier, R. D.; Thomann, R.; Kressler, J.; Mülhaupt, R.; Rudolf, B. *J. Polym. Sci. B: Polym. Phys*. **1997**, *35*, 1135.
(42) Doruker, P.; Mattice, W. L. *Macromolecules* **1997**, *30*, 5520.
(43) Abe, A.; Jernigan, R. L.; Flory, P. J. *J. Am. Chem. Soc*. **1966**, *88*, 631.
(44) Cho, J.; Mattice, W. L. *Macromolecules* **1997**, *30*, 637.
(45) Doruker, P.; Mattice, W. L. *Macromol. Symp*. **1998**, *133*, 47.
(46) Vao-soongnern, V.; Doruker, P.; Mattice, W. L. *Macromol. Theory Simul*. **2000**, *9*, 1.
(47) Xu, G.; Mattice, W. L. *Comput. Theor. Polym. Sci*. **2001**, *11*, 405.
(48) Akten, E. D.; Mattice, W. L. *Macromolecules* **2001**, *34*, 3389.
(49) Mandelkern, L.; Alamo, R. G. In *Polymer Data Handbook*; Mark, J. E., Ed.; Oxford University Press: New York, 1999; p 501.
(50) Widom, B. *J. Chem. Phys*. **1963**, *39*, 2808.
(51) Siepmann, J. I.; Frenkel, D. *Mol. Phys*. **1992**, *75*, 59.
(52) Spyriouni, T.; Economou, I. G.; Theodorou, D. N. *Macromolecules* **1997**, *30*, 4744.
(53) von Meerwall, E.; Beckman, S.; Jang, J.; Mattice, W. L. *J. Chem. Phys*. **1998**, *108*, 4299.
(54) Owen, M. J. In *Physical Properties of Polymers Handbook*; Mark, J. E., Ed.; American Institute of Physics: Woodbury, New York, 1996; p 669.
(55) LeGrand, D. G.; Gaines, G. L., Jr. *J. Colloid Interface Sci*. **1969**, *31*, 162.
(56) Heinbuch, U.; Fischer, J. *Mol. Simul*. **1987**, *1*, 109.